ELSEVIER

Journal of Power Sources 87 (2000) 12–20

JOURNAL OF POWER SOURCES

www.elsevier.com/locate/jpowsour

A review of state-of-charge indication of batteries by means of a.c. impedance measurements

Shalini Rodrigues [a], N. Munichandraiah [b,*], A.K. Shukla [a]

[a] *Solid State and Structural Chemistry Unit, Indian Institute of Science, Bangalore 560012, India*
[b] *Department of Inorganic and Physical Chemistry, Indian Institute of Science, Bangalore 560012, India*

Received 1 June 1999; accepted 4 August 1999

Abstract

A non-destructive estimation of the state-of-charge (SoC) of batteries facilitates optimum utilization of the battery for a given application, as well as evaluation of its state-of-health. Among various methods, a.c. impedance spectroscopy over a wide range of frequencies provides a variety of parameters which are functions of the SoC of a given battery. These parameters and their variation with SoC depend on the type of battery and on the experimental conditions. The impedance data of sealed commercial cells are rather tedious to analyze since the results are generally the combined parameters of both the positive and the negative electrodes. Separation of the parameters which correspond to the individual electrodes involves assumptions, the validity of which is open to question. Nevertheless, systematic linear and reproducible variations of measurable or computable impedance parameters with battery condition are useful indicators of the SoC in a non-destructive way. The present review consolidates the literature on the prediction of the SoC of batteries by means of a.c. impedance measurements.

Keywords: a.c. impedance; State-of-charge; Primary batteries; Secondary batteries

1. Introduction

The non-destructive evaluation of the available capacity of primary and secondary cells (or, batteries) has been the subject of much investigation. The ratio of the available capacity of a cell to its maximum attainable capacity is usually referred to as the state-of-charge (SoC) of the cell. An estimation of SoC facilitates optimum utilization of a battery for a given application, as well as an evaluation of its state of health.

Among the techniques which have been employed, a.c. impedance measurements provide knowledge of several parameters, the magnitudes of which may depend on the SoC of the cell. The first impedance measurements of batteries appear to have been made by Willihnganz in 1941 [1]. These involved excitation of the electrochemical cell by an a.c. voltage of small amplitude (about 5 mV) and evaluation of the resistive and the reactive components, or other related parameters such as the modulus of impedance and phase angle. As such measurements encompass a wide range of a.c. signal frequencies, various characteristic parameters of the electrochemical cell and the kinetics of the associated reactions can be evaluated.

The data of sealed commercial cells or batteries are rather tedious to analyze since the results are generally combined parameters of both the positive and the negative electrodes. Separation of the parameters corresponding to the individual electrodes involves assumptions, the validity of which is open to question. A direct estimation of the individual electrode parameters is not accessible since a suitable reference electrode cannot be introduced into a commercial sealed cell.

A study of the literature suggests that different parameters are shown useful for SoC evaluation of different battery systems under different experimental conditions. Hampson et al. [2] reviewed briefly the literature on impedance studies of batteries for the period up to 1980 and later Huet [3] surveyed the data for lead–acid and Ni–Cd secondary batteries. There does not appear to be any other examination of the prediction of SoC of batteries using impedance parameters.

In the present paper, it is intended to provide a comprehensive review of the literature on these impedance param-

* Corresponding author. Tel.: +91-80-309-2825; fax: +91-80-334-1683; e-mail: muni@ipc.iisc.ernet.in

0378-7753/00/$ - see front matter
PII: S0378-7753(99)00351-1

eters which indicate the SoC of batteries. A considerable number of studies have been made on several aspects of the impedance of batteries and battery electrodes. This review, however, only addresses published data for SoC predictions of primary and secondary batteries on the basis of a.c. impedance measurements.

2. Phenomenology

An electrochemical cell comprises resistive, capacitive and inductive components. The resistive components originate from the current-collectors, electrolyte, bulk of the electrode materials, electron-transfer reactions at the electrode/electrolyte interfaces, etc. The capacitive components are due to the double-layer capacitance. Inductive components usually arise from the porous nature of the electrodes. The measured total impedance of a cell is comprised of the resistive and the reactive components of the individual processes, which may be represented by an appropriate analogue known as an electrical equivalent circuit.

The positive and negative electrodes of a battery are characterized by the respective electrochemical reactions at equilibrium. Considering a typical electron-transfer reaction at an electrode, viz.,

$$\mathrm{O} + n\mathrm{e}^- = \mathrm{R} \tag{1}$$

the current density (i) and overpotential (η) are related by the Butler–Volmer equation, i.e.,

$$i = i_\mathrm{o}(\mathrm{e}^{-\alpha nF\eta/RT} - \mathrm{e}^{(1-\alpha)nF\eta/RT}) \tag{2}$$

where i_o is the exchange current density, α is the energy-transfer coefficient, and the other symbols have their usual meanings. When the cell is excited by an a.c. signal of about 5 mV peak-to-peak, Eq. (1) can be approximated to:

$$i = i_\mathrm{o} RT\eta/nF \tag{3}$$

On differentiation of Eq. (3), we get:

$$(\mathrm{d}\eta/\mathrm{d}i) = R_\mathrm{ct} = RT/nFi_\mathrm{o} \tag{4}$$

where R_ct is the charge-transfer resistance.

When a low frequency a.c. signal is impressed, a time-dependent diffusion layer is created. As no net current flows, a steady state is set up after a few cycles. The overall impedance (Z) consisting of contributions from diffusion and charge-transfer resistance can be expressed as [4]:

$$Z = R_\mathrm{ct} + \sigma/\omega^{1/2} + \sigma/j\omega^{1/2} \tag{5}$$

where σ is the Warburg coefficient. In the case of planar diffusion, σ is defined as:

$$\sigma = \frac{RT}{2^{1/2}n^2F^2AD^{1/2}}\left(\frac{1}{C_\mathrm{O}^\circ} + \frac{1}{C_\mathrm{R}^\circ}\right) \tag{6}$$

where A is the electrode area; D is the diffusion coefficient; C_O° and C_R° are the bulk concentrations of O and R, respectively. The frequency-dependent reactance due to diffusion, which includes the last two terms in Eq. (5) is known as the Warburg impedance (W).

Independent of the faradaic reaction, the electrode/electrolyte interface is characterized by another important parameter, namely, the double-layer capacitance (C_dl). The parameters R_ct and C_dl are considered to be in parallel. The impedance (Z) of the system is due to R_ct and C_dl, i.e.,

$$1/Z = (1/R_\mathrm{ct}) + j\omega C_\mathrm{dl} \tag{7}$$

In complex plane impedance analysis, a plot of the real part (Z') vs. the imaginary part $(-Z'')$ measured at several values of a.c. frequency takes the shape of a semicircle. At low frequencies, the impedance is purely resistive, because the reactance of C_dl is very large. At high frequencies, on the other hand, the reactance of C_dl is negligibly small and, therefore, the impedance approaches zero. Thus, the diameter of the semicircle, or the low frequency intercept on the real axis, provides the value of R_ct. The double-layer capacitance (C_dl) can be calculated from the a.c. frequency (f') corresponding to the maximum of Z'' on the semicircle as:

$$C_\mathrm{dl} = 1/2\pi f' R_\mathrm{ct} \tag{8}$$

During the course of discharge of a battery, the concentrations of species involved in the electrochemical reactions at both the electrodes vary with the time of discharge. Since the parameters i_o and σ depend on the concentrations, an estimation of impedance parameters is expected to provide an indication of the SoC of the battery.

The electrical equivalent-circuit of a battery represents the electrochemical processes occurring at the positive electrode (cathode), the negative electrode (anode), and in the electrolyte, as shown in Fig. 1. The significance of various circuit elements may be explained as follows (Fig. 1a). The battery electrodes are usually porous and the porosity of the electrodes leads to the impedance becoming inductive at high frequencies [2]. Therefore, L_a and L_c refer to inductors associated with the anode and the cathode, respectively. R_Ω refers to the ohmic resistance of the cell and includes the resistances of the electrolyte, electrode substrate metal, electrode leads, terminals, etc. The charge-transfer resistance $(R_\mathrm{a}, R_\mathrm{c})$, the double-layer capacitance $(C_\mathrm{a}, C_\mathrm{c})$ and the Warburg impedance $(W_\mathrm{a}, W_\mathrm{c})$ of the respective anode and the cathode are included in the circuit and follow Randles equivalent-circuit model.

For an equivalent circuit of a two-terminal storage battery (Fig. 1a), the impedance spectrum is expected to reflect the resistive, inductive, capacitive and Warburg components of the anode and cathode separately. It may be possible to observe this in an experimental spectrum, provided the magnitude of the time constants (RC) corre-

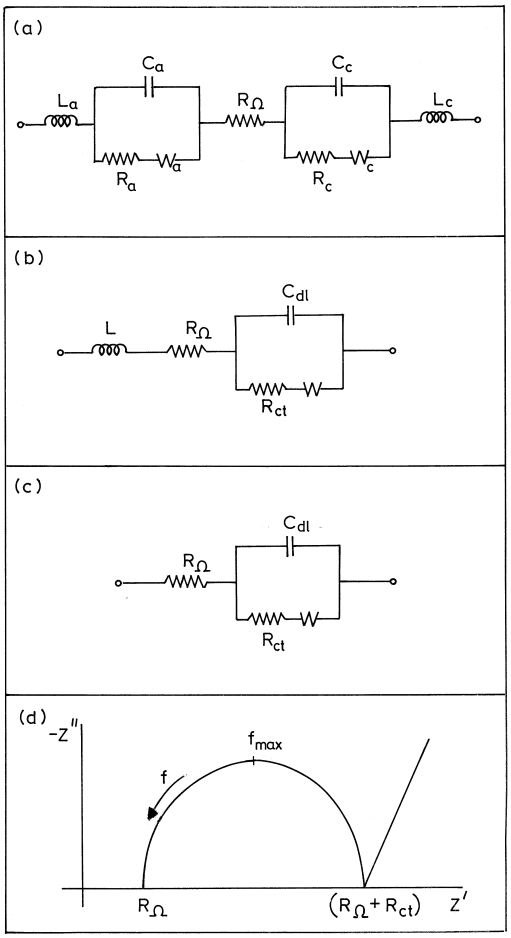

Fig. 1. (a) Equivalent circuit of two-terminal energy-storage cell with individual electrode-parameters. *L*, *C*, *R* and *W* refer to inductance, double-layer capacitance, charge-transfer resistance and Warburg impedance, respectively. Subscripts a and c refer to the anode and cathode. R_Ω is the ohmic resistance. (b) Equivalent circuit with combined parameters of the cell. R_{ct}, C_{dl} and *W* refer to charge-transfer resistance, double-layer capacitance and Warburg impedance, respectively. (c) Equivalent circuit as in (b) but without inductance. (d) Schematic complex-plane impedance spectrum corresponding to equivalent circuit shown in (c).

sponding to the anode and the cathode differ appreciably. In general, the total resistance of an energy storage cell is very low, and the parameters of the anode and the cathode are comparable in magnitudes. As a result, the impedance spectrum corresponding to the individual electrode parameters may not be clearly resolved, but it may represent the cell as a whole. The equivalent circuit may, therefore, be reduced as shown in Fig. 1b, where the combined parameters of the cell are shown [5]. As the inductance offers reactance at high a.c. frequencies, and if the experiments are carried out at low frequencies, the contribution of inductance to the cell impedance becomes negligibly small. Under these conditions, the inductance (L) may be omitted from Fig. 1b and the equivalent circuit reduces further to the one shown in Fig. 1c. The complex plane diagram of the impedance spectrum corresponding to the simplified equivalent circuit contains a semicircle and a linear spike as shown in Fig. 1d. The high frequency intercept of the semi-circle provides the value of R_Ω, the low-frequency intercept gives the value of charge-transfer resistance (R_{ct}). The double-layer capacitance (C_{dl}) and the Warburg coefficient can be calculated from f' and the linear spike, respectively.

3. Primary batteries

3.1. Zinc / manganese dioxide cells

Gopikanth and Satyanarayama [6] measured a.c. impedance of commercial Zn/MnO_2 cells of D-size at different SoC by employing a bridge technique. A lock-in-amplifier was used as the null detector to balance the bridge. The resistive and capacitive components were measured up to a frequency of 1 kHz. Although the bridge could not be balanced due to an inductive reactance of the cells at higher frequencies, a correlation of the impedance parameters with SoC was attempted below 300 Hz.

The impedance data of a Zn/MnO_2 cell in a complex plane diagram showed that there was a progressive change from semicircle behaviour at SoC ~ 1 to linear behaviour at SoC ~ 0. Thus, it was inferred that the electrochemical reactions occurred under charge-transfer control at high SoC values and they gradually changed to diffusion control with discharge of the cell. Although it was shown that there was a progressive change from charge-transfer control to diffusion-control with decrease in SoC of the Zn/MnO_2 cell, it was stated that when the impedance parameters (equivalent series/parallel resistance and capacitance, modulus of impedance, phase shift, etc.) were plotted against SoC, there were large fluctuations. The dependence of the impedance parameters on SoC was chaotic and none of the parameters were found useful as SoC indicators. The fluctuations in the values of the parameters were attributed to formation of a protective film on the zinc anode. The data of the complex plane impedance plots, which showed a progressive change from semicircular to linear behaviour, are in contradiction with the observation that the impedance parameters exhibit chaotic dependence on SoC. Since the dependence of the impedance parameters on SoC was not presented, it is not possible to analyze the observations. Additionally, it is not clear why the progressive change in impedance from semicircular to linear behaviour was not utilized for SoC prediction of Zn/MnO_2 batteries.

Karunathilaka and Hampson [7] measured the impedance of commercial Zn/MnO_2 Leclanche cells in the frequency range 0.1 mHz–10 kHz using a frequency response analyzer. The complex plane representation of the impedance data was comprised of a high frequency semicircle and a low frequency linear diffusion spike, as shown in Fig. 2. Since the semicircle was distorted and the measured values

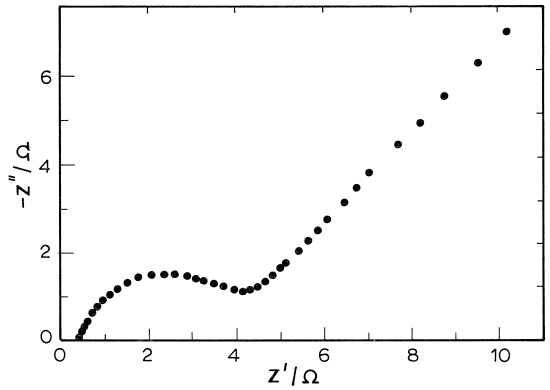

Fig. 2. Complex plane impedance plot of Zn/MnO_2 cell [7].

of capacitance were lower than the estimated values, the Randles equivalent circuit was modified by including an additional $R–C$ network and the individual impedance parameters were estimated by the method of least squares. It was found that the charge-transfer resistance and the Warburg coefficient of high surface area MnO_2 cathode were very small and the corresponding double-layer capacitance very large. As a result, the impedance of the zinc anode was the essential constituent of the measured cell impedance. Impedance measurements at different SoC values suggested that the impedance changed on discharging the cell. Although the form of the complex plane plot was broadly the same throughout and the diameter of the semicircle did not change significantly, the precise details of the shape altered as the cell was progressively drained. The high-frequency intercept on the real axis progressively increased throughout the discharge range, which was attributed to deposition of ZnO on the negative electrode. The change was, however, small. The low frequency tail of the complex plane plot, originally at 45° to the real axis for a fully charged cell, decreased to significantly lower angles as discharging continued. It approached a limit of $\pi/8$ at a discharge level of around 60%. In order to develop a SoC meter, an attempt was made to identify the most useful parameters, i.e., those which exerted strong influence on cell SoC. The criteria used were for the parameters that provided the most significant change with least dispersion in the SoC range 1–0.9. It was found that the capacitive reactance (R_x) at 31.2 Hz provided the best straight line when plotted against SoC. The value of R_x decreased by about 50% in between 1.0 and 0.9 SoC, as shown in Fig. 3. Based on these results, a SoC meter was developed and tested [8].

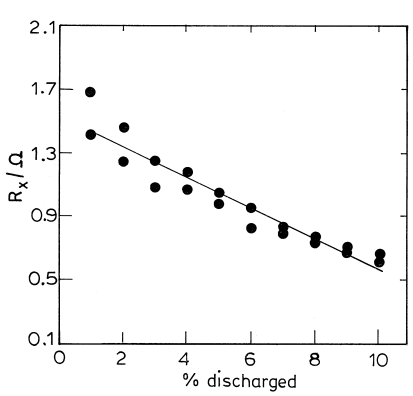

Fig. 3. Variation of capacitive reactance (R_x) of Zn/MnO_2 cell with discharge capacity [8].

3.2. Magnesium / manganese dioxide cell

Gopikanth and Satyanarayana [6] reported the impedance behaviour of Mg/MnO_2 cells at several SoC values. The complex plane impedance plot of an undischarged cell was linear and nearly parallel to the imaginary axis and, therefore, suggested capacitive behaviour of the cell. At SoC values ≤ 0.9, the impedance data were semicircles which indicate charge-transfer control of the electrochemical processes. The transition from capacitive behaviour at SoC ~ 1 to semicircular behaviour at SoC $\leq$ 0.9 was attributed to a break-down of the surface passive film on the magnesium anode due to passage of current through the cell. As observed with Zn/MnO_2 cells, the dependence of impedance parameters of the Mg/MnO_2 cells on SoC also involved large fluctuations. These were attributed to film break-down and reformation processes.

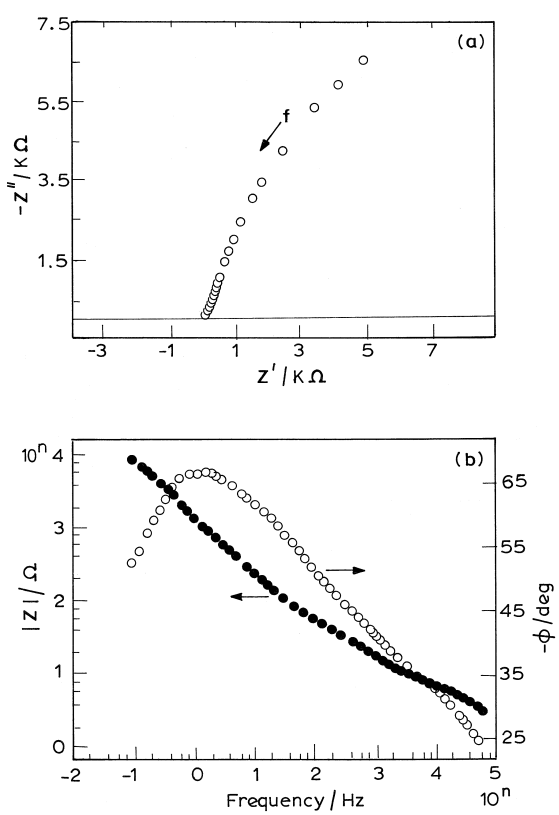

Fig. 4. Impedance spectrum of decade-aged Mg/MnO_2 cell. (a) Nyquist plot of imaginary part (Z'') vs. real part (Z'); (b) Bode plot of modulus of impedance (Z) and phase angle (ϕ) as a function of frequency [9].

Recently, we have investigated [9] the impedance behaviour of decade-aged Mg/MnO_2 cells, which retained their original capacity and were free from corrosion-induced electrolyte leaks. As reported earlier [6], the impedance of undischarged Mg/MnO_2 cells was capacitive in nature (Fig. 4). The internal resistance of a CD-size cell was as high as 10 kΩ, and this was attributed to the growth of the passive film during more than 10 years of ageing of the cells. Subsequent to discharge of the cells, the impedance decreased to a value as low as 140 Ω at a SoC ~ 0.9. The impedance spectrum of a partially discharged Mg/MnO_2 cell (SoC ≤ 0.7) contained two capacitive semicircles in the high frequency range and an inductive semicircle in the low frequency range. The two capacitive semicircles were attributed to the surface film resistance, the charge-transfer resistance of the magnesium corrosion process and the corresponding parallel capacitances. Plots of several impedance parameters as a function of all SoC display non-linear dependence (Fig. 5). This suggests that these parameters are of limited use for SoC or depth-of-discharge monitoring of Mg/MnO_2 cells. It was shown, however, that the frequency maximum of the high frequency semicircle had a linear dependence on SoC (Fig. 5).

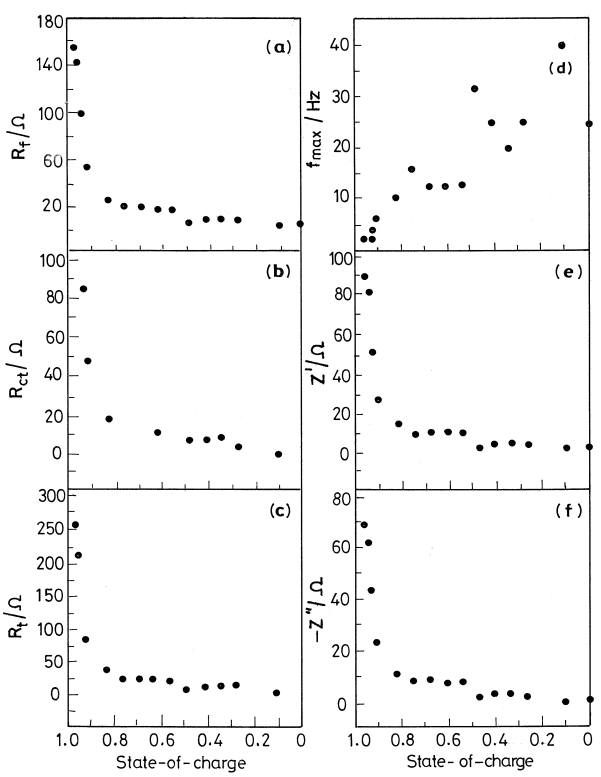

Fig. 5. Variation of impedance parameters with SoC of Mg/MnO_2 cell. R_f = surface film resistance; R_{ct} = charge-transfer resistance of corrosion of Mg; R_t = total cell resistance; f_{max} = frequency corresponding to maximum imaginary part of high-frequency semicircle; Z' = real part corresponding to f_{max}; Z'' = imaginary part corresponding to f_{max} [9].

4. Secondary batteries

4.1. Lead–acid cells

Keddam et al. [10] used a transfer function analyzer to measure the impedance of lead–acid batteries. Since the batteries had very low internal impedances, experiments were conducted by controlling the current. The impedance of Pb–acid batteries at a fully charged state, a partially discharged state and a completely discharged state were measured in the a.c. frequency range 10 kHz–1 mHz. Experiments were also conducted by using a reference electrode and the impedances of both positive and negative electrodes were measured. It was found that variations in the impedance were spread over a wide range of frequency. Nevertheless, a marked change in impedance with SoC was found in the low frequency range (≤ 1 Hz). Since the time constants of the processes occurring at the positive and negative electrodes were not very different, it was suggested that impedance measurements must be made on each plate in order to investigate the kinetics of the electrochemical processes of the individual electrodes.

Gopikanth and Satyanarayana [11] studied the impedance of lead–acid cells of 7 A h capacity using an a.c. bridge method. Either series resistance (R_s) and series capacitance (C_s) or parallel resistance (R_p) and parallel capacitance (C_p) of the cell were measured depending on either a series or parallel configuration of the balancing arm of the bridge. The modulus of impedance (Z) and the phase shift (ϕ) were calculated. At a.c. frequencies higher than 200 Hz, the inductive reactance of the cells became prominent, which was attributed to the porous structure of the electrodes. For the purpose of correlation between SoC, the lead–acid cell and the impedance parameters, the measurements were restricted to a.c. frequency values of less than 100 Hz.

The dependence of R_s, R_p and Z on the SoC of the lead–acid cell revealed that the magnitude of these parameters increased marginally at the end of discharge, while their variations at SoC values between 1.0 and 0.2 were negligible. The same type of dependence of these parameters on SoC were observed at all a.c. frequencies. On the other hand, C_p showed a flat minimum and C_s a broad maximum at SoC values of about 0.5. There was an approximately parabolic variation of ϕ with SoC with a minimum at a value of about 0.5. Because of the non-linear dependence of the impedance parameters on the SoC, the use of these parameters for prediction of the SoC of lead–acid batteries is considered to be limited.

On the contrary to the conclusions of Gopikanth and Satyanarayana [11], the results of Viswanathan et al. [12] suggested that impedance parameters could be useful for the prediction of the SoC of lead–acid batteries. Several 4- and 6-V batteries with capacities ranging from 3 to 9 A h were subjected to a.c. impedance measurements in the

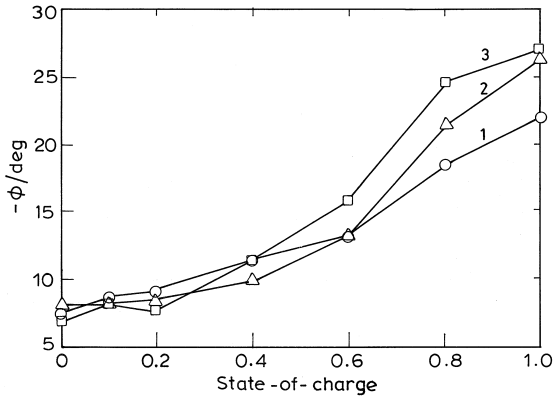

Fig. 6. Phase angle (ϕ) at 0.9 (1), 2.1 (2) and 5.9 Hz (3) vs. SoC of lead–acid cell [12].

frequency range 0.01–631 Hz at different SoC values. The Nyquist spectrum consisted of a depressed semicircle at high frequency and a Warburg linear spike at low frequency. The equivalent series capacitance (C_s) as a function of SoC passed through a maximum, thus, C_s was found to be unsuitable for SoC evaluation. On the other hand, the phase angle (ϕ) at frequencies < 0.9 Hz increased with increase in the SoC of lead–acid batteries (Fig. 6). The results demonstrated the advantage of obtaining impedance spectra over a wide range of frequency. As with the dependence of ϕ on SoC, the parameters C_s and equivalent parallel capacitance (C_p) were also found to be sensitive to the SoC in the low a.c. frequency range. The imaginary component passed through a minimum and, hence, was not suitable for SoC estimation. A complete tabulation of the impedance parameters at various frequencies as a function of the SoC enabled determination of the SoC of the lead–acid batteries, since a monotonically increasing or decreasing relationship was obtained at certain frequencies.

4.2. Nickel–cadmium cells

Satyanarayana et al. [5] examined the a.c. impedance characteristics of 4-A h capacity nickel–cadmium cells of the sintered plate and pressure-vented design over a wide range of frequencies and several SoC values. The parallel resistance (R_p) and parallel capacitance (C_p) obtained by means of a balancing bridge method were converted to equivalent series resistance (R_s), series capacitance (C_s) and a.c. phase shift (ϕ) using Eqs. 9 and 10.

The impedance data were analyzed using a uniform transmission-line analog model that consisted of long cylindrical pores in which diffusion of ions occurs along the axis of the pores whereas both diffusion and charge-transfer reactions occur at the interface between the pore wall and active material. It was observed that the internal resistance of the nickel–cadmium cells was mainly due to the combined resistance of the electrolyte and the inter-electrode separator. The resistance components, therefore, were not useful for predicting the SoC of the cells. On the other hand, C_p, C_s and ϕ when measured at low a.c. frequencies, were shown to vary in a way that was useful for the prediction of SoC, Fig. 7. A change in the double-layer capacitance at the pore wall/active material interface due to crystal nucleation and growth processes was identified as the factor which was underlying the correlation of these parameters with SoC of the nickel–cadmium cells.

Haak et al. [13] studied the impedance of 12-A h, space-quality, sealed nickel–cadmium cells for a non-destructive determination of cell life-time, in particular, the probability of premature failure. The impedance was measured in the 10 kHz–0.4 mHz frequency range as the cell was subjected to charge–discharge cycles at several temperatures and under different depth-of-discharge conditions. The complex plane plot of the impedance spectrum

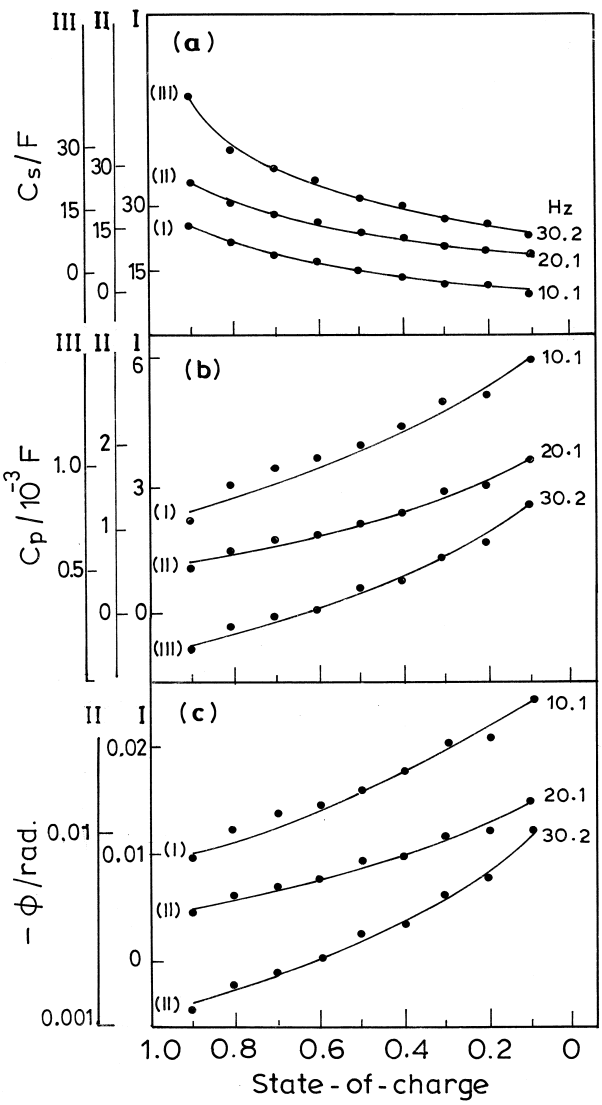

Fig. 7. (a) Equivalent series capacitance (C_s); (b) equivalent parallel capacitance (C_p); (c) phase angle (ϕ) vs. SoC of nickel–cadmium cell [5].

consisted of a depressed semicircle in the high frequency region followed by a linear spike in the low frequency region. The values of R_p, C_p and Warburg angle (θ) were evaluated for Ni–Cd cells in the fully discharged state over a large number of charge–discharge cycles. It was found that the value of θ increased steadily with cycle number. The other parameters pertaining to the high frequency region of the impedance, viz., R_p and C_p did not show a regular trend. It was, thus, suggested that a high or rapidly increasing value of θ could signal imminent cell failure. In view of the considerable interest in impedance measurements as a means to determine the SoC of the nickel–cadmium cells, the data were evaluated for incidental relationships with SoC. It was found that the slope in the low frequency region (m) of the log Z vs. log f Bode plot was a useful parameter. The value of m was shown to increase with SoC. The values of m, however, were presented for only three SoC values. An establishment of correlation between m and SoC could have been possible if m values were presented encompassing a wide range of SoC values.

Hughes et al. [14] employed 23 A h nickel–cadmium cells for impedance measurements and to identify suitable parameters for indication of the residual capacity in each cell. The complex plane plot of the impedance spectrum recorded in the frequency range 10 kHz–1 mHz consisted of a small inductive component and a capacitive component in which the loci make an angle of about 70° to the real axis. This inferred the presence of blocking films, which were due to cadmium hydroxide. A fully charged cell was subjected to impedance measurements over a period of 120 days and changes in the spectra were noticed at frequencies below 49 mHz. The changes, however, were not regular with time and therefore the data were not analyzed. The impedance data were deconvoluted to provide an accurate indication of the SoC of the cells. The data did not, however, readily match to a simple analogue circuit. As a result, a computer program was used to search the impedance data files for a possible parameter. At each SoC and at every frequency, the resistive, capacitive and inductive reactances and total impedance were calculated. The correlation coefficient of each of these components vs. SoC was calculated together with the slope and intercept. From the results of these analyses, the capacitive reactance at low frequencies (10–0.1 Hz) was identified as the appropriate parameter for prediction of SoC. The average capacitive reactance of six nickel–cadmium cells vs. SoC (Fig. 8) resulted in a straight line which extended the complete range of SoC and had a slope of about 130%/mΩ at 0.39 Hz.

Blanchard [15] studied the a.c. impedance of 0.85-A h, AA size, sealed nickel–cadmium cells and analyzed the data for identification of parameters which depend on SoC. Unlike the studies usually carried out with cells under potentiostatic non-zero current conditions, the experiments were performed when the cells were under charge or

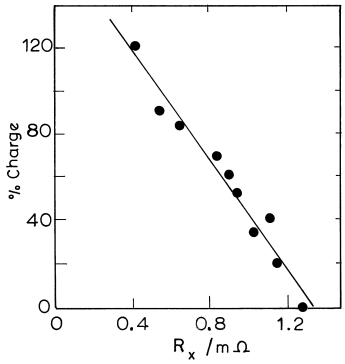

Fig. 8. Variation of capacitive reactance (R_x) at 0.3931 Hz with percent charge of nickel–cadmium cell [14].

discharge at the C rate (i.e., current flowing through the cell was 0.85 A). A few experiments at slower rates of charge or discharge were also reported. The complex plane diagrams were composed of two (during charge) or three (during discharge) capacitive loops. The high-frequency intercept, which provided the ohmic resistance of the cell (25–30 mΩ range), as well as the high frequency capacitive loop did not show dependence on the SoC of the nickel–cadmium cells. The low frequency (100–0.1 Hz range) capacitive loop was found useful for prediction of SoC. A fitting program was employed to evaluate the associated charge-transfer resistance (R_{ct}) and double-layer capacitance (C_{dl}). There was an increase in the value of R_{ct} as the SoC increased from 0 to 1. During overcharge of the cells, however, it decreased. The latter was attributed to the rise in temperature and the change from the main electrochemical reaction to a secondary reaction. Also, the value of C_{dl} increased from about 0.3 to 1.5 F during charge and overcharge. In addition to the variation of R_{ct} and C_{dl}, some techniques which allow determination of an approximate SoC were also proposed. For example, if the cell was under C-rate charge or discharge, by measuring the impedance modulus at 1 Hz it was possible to detect when the battery was fully charged if the measurements were carried out during charge, or when only 15%–20% of the initial capacity was still available if the measurements were carried out during discharge.

Viswanathan et al. [16] measured the impedance of commercial nickel–cadmium cells of capacity 1.8–2 A h at several SoC values using an experimental set-up which consisted of a lock-in-amplifier and a potentiostat that were driven by a computer. The complex-plane impedance diagram of the nickel–cadmium cells comprised a depressed capacitive semicircle in the high-frequency region and a linear diffusive part in the low-frequency region. The data were analyzed by means of an equivalent circuit curve fitting procedure. A constant phase element (Q) was considered in place of the capacitance. The modulus of the impedance ($|Z|$) as well as the phase angle (ϕ) at several low frequency values vs. cell SoC passed through minima. These parameters, therefore, were not considered useful

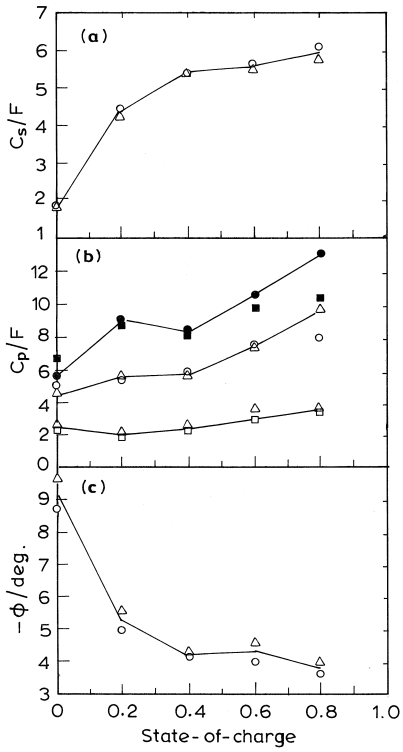

Fig. 9. (a) Equivalent series capacitance (C_s); (b) equivalent parallel capacitance (C_p); (c) phase angle (ϕ) vs. SoC of nickel–cadmium cell [16].

for prediction of SoC. The imaginary component of the impedance (Z'') also passed through a minimum and, hence, was not useful. The equivalent series capacitance (C_s) and the equivalent series resistance (R_s) were calculated using Eqs. 9 and 10 for low frequency values. It was shown that ϕ at 25 Hz decreased, C_s at 25 Hz increased, and C_p at 0.118–0.226 Hz increased with the SoC of the nickel–cadmium cells (Fig. 9). These parameters, therefore, shared promise for estimation of SoC.

4.3. Nickel–metal hydride cells

Bundy et al. [17] employed impedance spectroscopy for the prediction of the SoC of nickel–metal hydride cells at

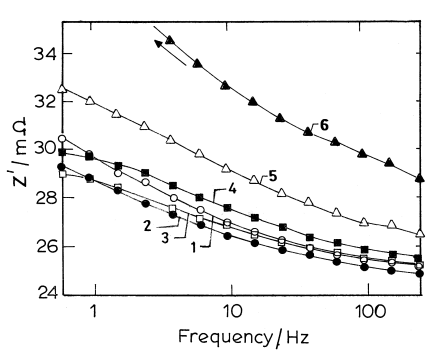

Fig. 10. Real part of impedance (Z') vs. frequency measured at SoC of 1.0 (1), 0.78 (2), 0.56 (3), 0.34 (4), 0.11 (5) and 0 (6) during discharge at 0.2 C rate [17].

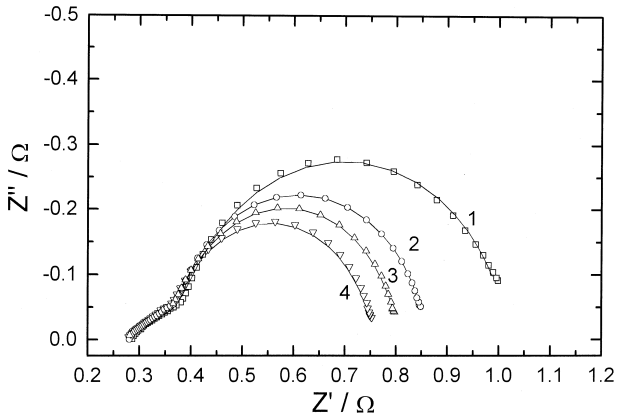

Fig. 11. Impedance spectra of lithium-ion battery at SoC ≈ 0 (1), 0.14 (2), 0.28 (3), 0.42 (4). Inductive data are omitted. Experimental data shown by symbols and theoretical data by solid lines [18].

both open-circuit and during discharge. Partial least squares regression was employed to analyze the data obtained under open-circuit conditions and during discharge at rates from 0.2 to 0.8 C by imposing an a.c. current signal. The complex-plane impedance spectrum was dependent on the SoC value. This dependence was shown to be more evident when the real part of the impedance was plotted against frequency at different SoC values. The real part decreased, especially at low frequencies, with increase in the SoC (Fig. 10). The impedance data were measured at several rates of cell discharge. Although there were significant differences, depending on the load, no clear-cut relationship could be established. The variations in the real part of the impedance for different loads were as large as the variations at SoC values between 0.3 and 1.0 at a constant load of 0.2 C. Owing to this difficulty, a statistical method involving a multivariate model was employed for predicting SoC for different discharge loads.

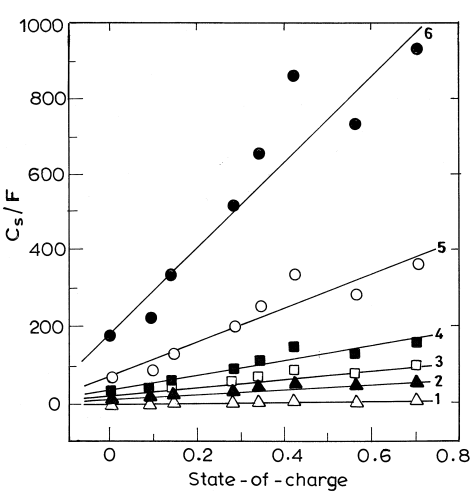

Fig. 12. Dependence of equivalent series capacitance (C_s) on SoC value of a battery at frequency (Hz) values of 0.5 (1), 0.1 (2), 0.08 (3), 0.06 (4), 0.04 (5), and 0.025 (6) [18].

4.4. Lithium cells

Recently, we have analyzed [18] the impedance of a 7.2-V, 1.25-A h sealed lithium-ion battery for estimation of the SoC. The complex-plane diagram of the impedance spectrum in the frequency range 100 kHz–25 mHz comprised an inductive loop in the high-frequency range and two capacitive semicircles. While the inductive loop was attributed to the porous nature of electrodes, the capacitive semicircles were related to the electrode process. The low-frequency capacitive semicircle was found to be sensitive to the SoC of the battery, as shown in Fig. 11. The data were analyzed by a non-linear least squares fitting procedure. The following impedance components were examined as functions of the SoC: ohmic resistance of the battery (R_Ω); parallel resistance (R_p) and constant phase element corresponding to the high frequency capacitive semicircle; parallel charge-transfer resistance (R_{ct}) and constant phase element corresponding to the low-frequency capacitive semicircle; frequency maximum and corresponding real (Z') as well as imaginary (Z'') components of the second semicircle; phase angle (ϕ) at several frequencies; equivalent series resistance (R_s) and equivalent series capacitance (C_s). Although some of the parameters were found to vary with the SoC, the equivalent series capacitance at 25 mHz exhibited a large and linear variation with SoC (Fig. 12). Thus, the impedance parameters derived from the low-frequency semicircle, in particular the equivalent series capacitance, proved helpful in predicting the SoC of the lithium-ion battery.

5. Conclusions

Reported studies of the prediction of the SoC of primary and secondary batteries using a.c. impedance parameters have been reviewed. Measurements of battery impedance under different conditions, viz., open-circuit potentiostatic, galvanostatic charge and discharge, during a wide range of charge–discharge cycles, are reported at different SoC values of the cells. In several publications, the impedance spectra reflect essentially the charge-transfer controlled electrode processes in the high a.c. frequency range and diffusion-controlled processes in the low-frequency region. While the charge-transfer behaviour is characterized by a semicircle, the diffusion behaviour is typified by a linear spike in the complex-plane impedance diagrams. Analysis of the data, either manually or by curve-fitting procedures, results in several impedance parameters which are functions of the battery SoC. The parameters, however, vary with the type of battery and the experimental conditions. Although the impedance parameters and their variations with SoC are not unique for all battery systems, it appears to be imperative to perform a wide range of impedance experiments for identification and use of impedance parameters for estimating the SoC of a given battery.

References

[1] E. Willihnganz, Trans. Am. Electrochem. Soc. 79 (1941) 253.
[2] N.A. Hampson, S.A.G.R. Karunathilaka, R. Leek, J. Appl. Electrochem. 10 (1980) 3.
[3] F. Huet, J. Power Sources 70 (1998) 59.
[4] R. Greef, R. Peat, L.M. Peter, D. Pletcher, J. Robinson, Instrumental Methods in Electrochemistry, Ellis Horwood, 1985, p. 251.
[5] S. Satyanarayana, S. Venugopalan, M.L. Gopikanth, J. Appl. Electrochem. 9 (1979) 125.
[6] M.L. Gopikanth, S. Satyanarayana, J. Appl. Electrochem. 9 (1979) 581.
[7] S.A.G.R. Karunathilaka, N.A. Hampson, J. Appl. Electrochem. 10 (1980) 357.
[8] S.A.G.R. Karunathilaka, N.A. Hampson, R. Leek, T.J. Sinclair, J. Appl. Electrochem. 10 (1980) 799.
[9] N. Munichandraiah, J. Appl. Electrochem. 29 (1999) 463.
[10] M. Keddam, Z. Stoynov, H. Takenouti, J. Appl. Electrochem. 7 (1977) 539.
[11] M.L. Gopikanth, S. Satyanarayana, J. Appl. Electrochem. 9 (1979) 369.
[12] V.V. Viswanathan, A.J. Salkind, J.J. Kelley, J.B. Ockerman, J. Appl. Electrochem. 25 (1995) 729.
[13] R. Haak, C. Ogden, D. Tench, S.D. Stefano, J. Power Sources 12 (1984) 289.
[14] M. Hughes, R.T. Barton, S.A.G.R. Karunathilaka, N.A. Hampson, R. Leek, J. Appl. Electrochem. 15 (1985) 129.
[15] Ph. Blanchard, J. Appl. Electrochem. 22 (1992) 1121.
[16] V.V. Viswanathan, A.J. Salkind, J.J. Kelley, J.B. Ockerman, J. Appl. Electrochem. 25 (1995) 716.
[17] K. Bundy, M. Karlsson, G. Lindbergh, A. Lundqvist, J. Power Sources 72 (1998) 118.
[18] R. Shalini, N. Munichandraiah, A.K. Shukla, J. Solid State Electrochem. 3 (1999) 397.